Synthesis, crystal structure, and thermal stability of double borate Na$_3$ErB$_2$O$_6$

Alexey K. Subanakov *, Evgeniy V. Kovtunets, Bair G. Bazarov, Jibzema G. Bazarova

Baikal Institute of Nature Management SB RAS, 670047 Sakhyanovoy st., 6, Ulan-Ude, Russia
*   Corresponding author: subanakov@binm.bscnet.ru

This article belongs to the regular issue.

Abstract

Double borate Na$_3$ErB$_2$O$_6$ was synthesized by the solid-state reaction. The crystal structure of Na$_3$ErB$_2$O$_6$ was refined by the Rietveld method: $P2_1/c$, a = 6.49775(14) Å, b = 8.50424(17) Å, c = 12.0067(3) Å, β = 118.4797(9)°, Z = 4. The crystal structure of Na$_3$ErB$_2$O$_6$ consists of –[ErO$_6$]$_\infty$-chains along the "b" axis, which are linked by BO$_3$ triangles in a three-dimensional framework. Sodium atoms occupy empty positions inside the channels. The thermal behavior of Na$_3$ErB$_2$O$_6$ was studied in detail in the range of 25–1150 °C range by DSC and TG methods. Na$_3$ErB$_2$O$_6$ congruently melts at 1116 °C. Based on the results of DSC measurements, three reversible phase transitions were found for Na$_3$ErB$_2$O$_6$.

1. Introduction

Borates are considered to be attractive functional materials for non-linear optic and luminescence due to their wide variety of crystal structures, low synthesis temperature, and environmental benignity [1–13]. Today commercially used nonlinear optical crystals of borates with superior optical properties are β-BaB$_2$O$_4$ [14] and LiB$_3$O$_5$ [15]. Recent studies of borates are related to birefringent materials [16] and self-frequency-doubling (SFD) laser ones [17]. SFD crystals belong to multi-functional materials and possess both laser and frequency doubling properties. The basic requirements for an efficient SFD laser crystal are excellent laser properties and excellent nonlinear optical properties with suitable birefringence. Therefore, SFD materials contained rare-earth elements and a nonlinear framework.

To search new SFD materials, the oxide systems based on alkaline, rare earth, and boron were extensively studied. Exploration of the Na$_2$O–R$_2$O–B$_2$O$_3$ systems revealed the existence of a number of double borates: Na$_2$R$_2$(BO$_3$)$_2$ [18–20], Na$_3$RB$_2$O$_6$ [21–23], Na$_3$R$_2$B$_3$O$_9$ [21,24–26], Na$_3$Y$_3$B$_4$O$_{12}$ [27], Na$_3$R$_9$O$_3$B$_8$O$_{24}$ [28,29]. Our attention was attracted by double borates with the general formula Na$_3$RB$_2$O$_6$. This family of compounds includes borates with large lanthanides such as Na$_3$LaB$_2$O$_6$ [21], Na$_3$PrB$_2$O$_6$ [22], Na$_3$SmB$_2$O$_6$ [22], Na$_3$EuB$_2$O$_6$ [22], Na$_3$YB$_2$O$_6$ [23] and Na$_3$GdB$_2$O$_6$ [23]. The subject of our study is the possibility of replacing large lanthanides with erbium. The crystal structure and thermal stability of double borate Na$_3$ErB$_2$O$_9$ was studied in the present work.

2. Experimental

The title compounds were prepared by solid state reactions using high purity starting reagents: Na$_2$CO$_3$ (99.8%, Sigma Aldrich Ltd.), Er$_2$O$_3$ (99.9%, Red Chemist, Ltd., Russia), and H$_3$BO$_3$ (99.5%, Sigma Aldrich Ltd.). Before weighing, Er$_2$O$_3$ had been preheated at 850 °C for 8 hours to remove absorbed water. The reagents were weighed on an analytical balance with an accuracy of 0.5 mg. The mixtures of Na$_2$CO$_3$, Er$_2$O$_3$, and H$_3$BO$_3$ at molar ratio 3:1:2 were thoroughly ground in an agate mortar, slowly heated up to 300 °C, and were kept for 5 hours. Then the samples were reground and annealed at 600 °C for 5 hours and finally at 700 °C for 40 hours with intermediate grindings until equilibrium was reached. Temperature was measured with a Pt–PtRh thermocouple. The temperatures up to 1200 °C were controlled with an accuracy of ±2 °C with an OMRON instrument. The equilibrium was considered to be reached only when two successive heat treatments resulted in identical X-ray diffraction patterns.

Powder X-ray diffraction data were recorded by a D8 ADVANCE Bruker AXS diffractometer (Vantec-1 detector) at room temperature using Cu Kα radiation and scanning

from $2\theta = 8°$ to $100°$ in increments of $0.02°$ and a counting time of 0.1 s/step. Phase purity was verified by powder X-ray diffraction (XRD) and the profile was compared to that reported for the isostructural phase $Na_3NdB_2O_6$.

The TOPAS 4.2 [30] software suite was used to analyze the experimental data and to perform the Rietveld refinement of the obtained compound. All peaks in the X-ray powder diffraction pattern for $Na_3ErB_2O_9$ were indexed satisfactory in a monoclinic cell (space group $P2_1/c$).

Differential scanning calorimetry (DSC) and thermogravimetric (TG) measurements were performed on an STA 449 F1 Jupiter thermoanalyzer (NETZSCH) in the temperature range of 30–1150 °C in argon flow. Pt crucibles were used as vessels. Pt–PtRh thermocouples were used for temperature measurement. The precision of temperature measurement was ±1 °C. The heating and cooling rates were 10 °C/min.

3. Results and discussion

The synthesized sample of $Na_3ErB_2O_6$ is pink powder, which is characteristic for the Er-containing oxides. The structure of $Na_3NdB_2O_6$ was used as initial model for the Rietveld refinement to define the positions of atoms. They were refined by isotropic approximation with "soft" limitations of the B–O distance and the B–O–B bond angles. The refined parameters were added sequentially with the graphical simulation of the background in continuous. The Pearson VII function was used to describe the shape of peaks. The isotropic displacement parameters (B_{iso}) for the Er and Na atoms were refined separately, while for the O and B atoms they were taken as equivalent. The refinement process included corrections for the sample preferred orientation and anisotropic broadening of peaks within the model of spherical harmonics.

The refinement was stable and gave low R-factors (Fig. 1, Table 1). $Na_3ErB_2O_6$ was crystallized in the monoclinic system with the space group $P2_1/c$. The unit cell parameters are: $a = 6.49775(14)$ Å, $b = 8.50424(17)$ Å, $c = 12.0067(3)$ Å, $\beta = 118.4797(9)°$, $Z = 4$. Coordinates of atoms are given in Table 2. Further details of the crystal structure may be obtained from supplementary material.

In the structure of $Na_3ErB_2O_6$ (Fig. 2a), Er atoms are coordinated by seven O atoms in a distorted pentagonal bipyramid. The bipyramids share corners, forming a zig-zag chain along the "b" direction, and the chain is reinforced by the $B1O_3$ group, which uses all its three B–O bonds to join the neighboring bipyramids (Fig. 2a). Along with the "a" and "c" directions, these chains are connected via the $B2O_3$ groups, thereby constructing a three-dimensional framework. Na1 and Na3 atoms are located in the interlayer channels and Na2 atom sits in the inlayer

empty positions (Fig. 2b–d). Three Na atoms are coordinated by seven, six, and four O atoms, respectively.

The main bond lengths (Å) and angles (°) of $Na_3ErB_2O_6$ are shown in Table 3.

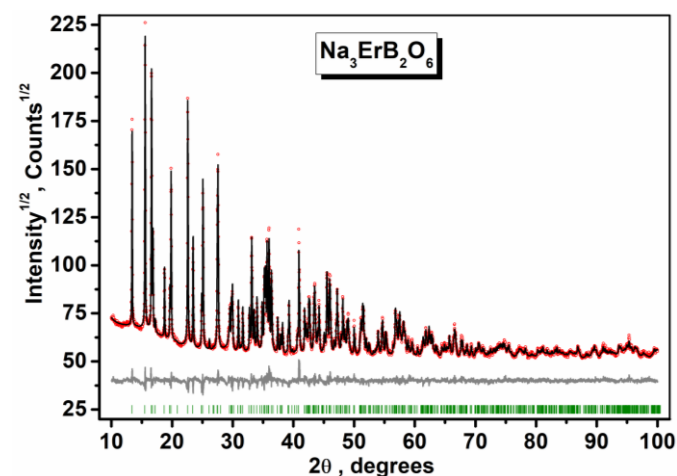**Fig. 1** XRD data for $Na_3ErB_2O_6$ refined by the Rietveld analysis: measured (red points), calculated (black profile) and difference between experimental points and calculated profile (grey curve)

Table 1 Crystallographic data for $Na_3ErB_2O_6$ phase at room temperature

Chemical formula	$Na_3ErB_2O_6$
Space group	$P2_1/c$ (14)
Formula weight, g/mol	353.9
Unit cell dimensions, Å $\alpha = \gamma = 90°$	$a = 6.49775(14)$ $b = 8.50424(17)$ $c = 12.0067(3)$ $\beta = 118.4797(9)°$
Cell volume, Å³	583.18(2)
Z	4
Calculated density (g/cm³)	4.163
R_p, %	2.571
R_{wp}, %	3.534
R_{exp}, %	1.572
Bragg R-factor, %	1.864
χ_2	2.249

Table 2 Fractional atomic coordinates and isotropic or equivalent isotropic displacement parameters of $Na_3ErB_2O_6$ structure

	x	y	z	$B_{iso}*/B_{eq}$
Er	0.0970(3)	0.1261(1)	0.3287(1)	0.9(2)
Na1	0.380(2)	0.8039(8)	0.3841(7)	1.1(3)
Na2	0.058(2)	0.2963(8)	0.0802(8)	0.9(3)
Na3	0.331(2)	0.9488(8)	0.1134(7)	3.1(3)
B1	0.139(3)	0.4379(7)	0.3695(8)	1.0(6)
B2	0.351(1)	0.5864(8)	0.1209(5)	1.0(6)
O1	0.255(2)	0.334(1)	0.4714(9)	0.5(2)
O2	0.049(2)	0.373(2)	0.2513(7)	0.5(2)
O3	0.137(2)	0.600(1)	0.3911(9)	0.5(2)
O4	0.226(1)	0.674(1)	0.1611(5)	0.5(2)
O5	0.251(2)	0.505(1)	0.0086(7)	0.5(2)
O6	0.413(1)	0.080(1)	0.3075(5)	0.5(2)

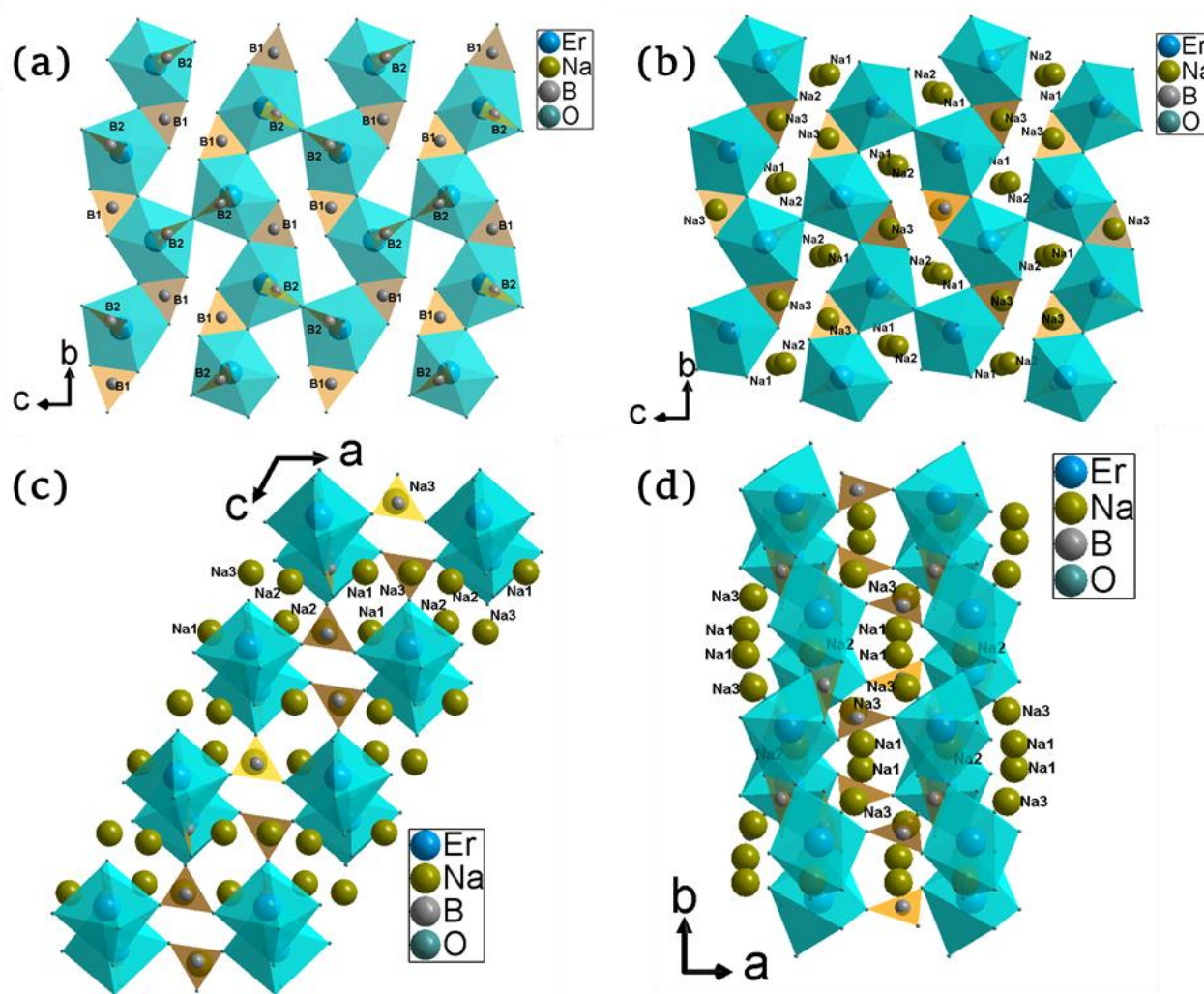**Fig. 2** The crystal structure of $Na_3RB_2O_9$: a, b) ErO_7 chains, BO_3 triangles (a) and Na atoms (b) along *a* axis; b, c) a general view along *b* and *c* axes

The DSC curves recorded for $Na_3ErB_2O_6$ are shown in Fig. 3. Four endothermic signals at 717, 907, 1014, and 1116 °C were detected during the sample's first heating, as shown in Fig. 3. The endothermic peak at 1116 °C corresponds to the melting point of $Na_3ErB_2O_6$. The X-ray diffraction measurements indicate the congruent melting of the borate (Fig. 4). To determine the nature of the endothermal effects at 717, 907, 1014 °C and prove congruent melting, the same sample was recorded in the "heating-cooling" mode over the temperature range of 100–1150 °C (with melting). At first cooling, $Na_3ErB_2O_6$ shows exothermic effects at 712, 831, 1000, 1098 °C. The second cooling reveals a new exothermic effect at 706 °C that seems to correspond to $Na_3ErB_2O_6$ partial decomposition, which is confirmed by X-ray analysis. The observed temperatures hystereses are about 5, 76, 14, 18 degrees. Thus, the signature observed at 600–1150 °C reveals the existence of reversible phase transitions (type I) in $Na_3ErB_2O_6$ and, respectively, additional experiments are needed to define the structure of the high-temperature modification of β, γ – $Na_3ErB_2O_6$.

Table 3 Main bond lengths (Å) and angles (°) of $Na_3ErB_2O_6$

Er—O1	2.33(1)	Na2—O5	2.55(1)
Er—O2^i	2.36(1)	Na2—O6	3.19(1)
Er—O2	2.26(2)	Na3—O1^x	2.40(1)
Er—O3^i	2.32(1)	Na3—O3^x	2.38(1)
Er—O4^i	2.20(1)	Na3—O4	2.57(1)
Er—O5^{ii}	2.20(1)	Na3—O6^{vii}	2.40(1)
Er—O6	2.22(1)	B1—O1	1.40(1)
Na1—O1^{iii}	2.50(1)	B1—O2	1.37(1)
Na1—O2^{iv}	2.53(1)	B1—O3	1.40(1)
Na1—O3	2.38(1)	B2—O4	1.35(1)
Na1—O4	2.61(1)	B2—O5	1.37(1)
Na1—O5^v	2.72(1)	B2—O6^v	1.36(1)
Na1—O5^{vi}	2.60(1)	O1—B1—O2	116(1)
Na1—O6^{vii}	2.56(1)	O1—B1—O3	120(1)
Na2—O1^{viii}	2.48(1)	O2—B1—O3	123(1)
Na2—O2	2.18(1)	O4—B2—O5	123(7)
Na2—O3^i	2.22(1)	O4—B2—O6^v	120(5)
Na2—O4^{ix}	2.60(1)	O5—B2—O6^v	118(1)
Na2—O5^{ix}	2.44(1)		

Symmetry codes: (i) $-x$, $y-1/2$, $-z+1/2$; (ii) x, $-y+1/2$, $z+1/2$; (iii) $-x+1$, $-y+1$, $-z+1$; (iv) $-x$, $y+1/2$, $-z+1/2$; (v) $-x+1$, $y+1/2$, $-z+1/2$; (vi) x, $-y+3/2$, $z+1/2$; (vii) x, $y+1$, z; (viii) x, $-y+1/2$, $z-1/2$; (ix) $-x$, $-y+1$, $-z$; (x) x, $-y+3/2$, $z-1/2$.

It should be pointed out that the transition was not found in $Na_3RB_2O_6$ (R = Pr, Sm, Eu) [22]. Respectively, it can be reasonably assumed that the appearance of the phase transitions is observed only for the $Na_3RB_2O_6$ borates where rare earth elements have small ionic radius.

An X-ray examination of solid-state interactions between the components of the $Na_2O–Er_2O_3–B_2O_3$ system resulted in finding double borate $Na_3ErB_2O_6$. $Na_3ErB_2O_6$ was synthesized by solid-state reaction. The crystal structure of $Na_3ErB_2O_6$ was refined by the Rietveld analysis. $Na_3ErB_2O_6$ consists of ErO_7 distorted pentagonal bipyramids and BO_3 groups. $Na_3ErB_2O_6$ congruently melts at 1116 °C. The DSC and TG experiments assume that after melting $Na_3ErB_2O_6$ decomposing with formation of Er_2O_3. The observed endothermic effects on the DSC curve are assumed to be attributed to high-temperature phase transitions of the title compound. This assumption prompts us to thoroughly investigate this family of compounds in the future.
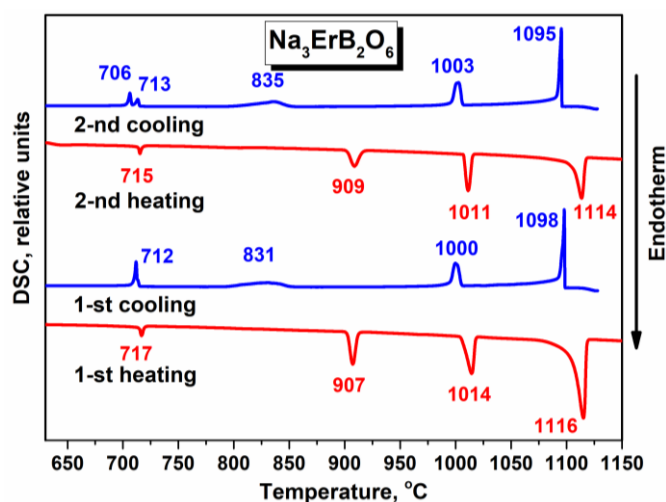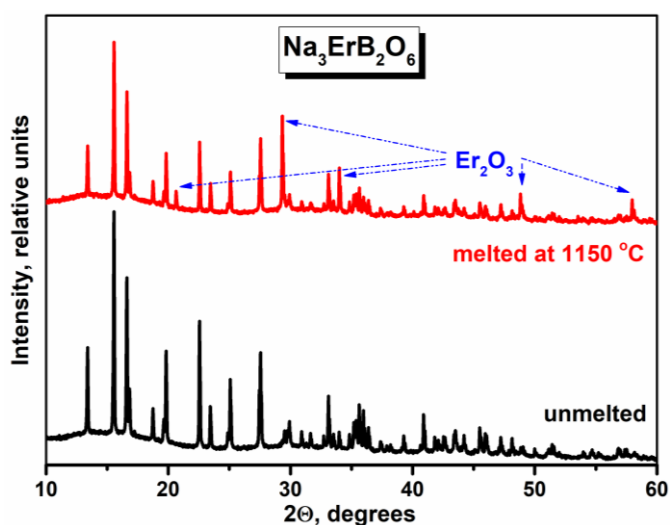

Fig. 3 DSC measurement results

Fig. 4 X-ray patterns of unmelted and melted $Na_3ErB_2O_6$ specimen

Conclusions

An X-ray examination of solid-state interactions between the components of the $Na_2O–Er_2O_3–B_2O_3$ system resulted in finding the double borate, $Na_3ErB_2O_6$. $Na_3ErB_2O_6$ was synthesized by solid-state reactions. The crystal structure of $Na_3ErB_2O_6$ was refined by the Rietveld analysis. $Na_3ErB_2O_6$ consists of ErO_7 distorted pentagonal bipyramids and BO_3 groups. $Na_3ErB_2O_6$ congruently melts at 1116 °C. The DSC and TG experiments demonstrated that after melting $Na_3ErB_2O_6$ decomposes with formation of Er_2O_3. The observed endothermic effects on the DSC curve are assumed to be attributed to high-temperature phase transitions of the title compound. This assumption prompts us to thoroughly investigate this family of compounds in the future.

Acknowledgments

References

1. Mutailipu M, Poeppelmeier KR, Pan S. Borates: A Rich Source for Optical Materials. Chem Rev. 2021;121:1130–1202. doi:10.1021/acs.chemrev.0c00796
2. Yang SH, Xue H, Guo SP. Borates as promising electrode materials for rechargeable batteries. Coord Chem Rev. 2021;427. doi:10.1016/j.ccr.2020.213551
3. Leonyuk NI, Maltsev VV, Volkova EA. Crystal chemistry of high-temperature borates. Molecules. 2020;25. doi:10.3390/MOLECULES25102450
4. Topnikova AP, Belokoneva EL. The structure and classification of complex borates. Russ Chem Rev. 2019;88:204–228. doi:10.1070/rcr4835
5. Mutailipu M, Zhang M, Yang Z, Pan S. Targeting the Next Generation of Deep-Ultraviolet Nonlinear Optical Materials: Expanding from Borates to Borate Fluorides to Fluorooxoborates. Acc Chem Res. 2019;52:791–801. doi:10.1021/acs.accounts.8b00649
6. Becker P. Borate materials in nonlinear optics. Adv Mater. 1998;10:979–992. doi:10.1002/(SICI)1521-4095(199809)10:13<979::AID-ADMA979>3.0.CO;2-N
7. Chen C, Wu Y, Li R. The development of new NLO crystals in the borate series. J Cryst Growth. 1990;99:790–798. doi:10.1016/S0022-0248(08)80028-0
8. Kovtunets EV, Subanakov AK, Bazarov BG. Synthesis, structure and luminescent properties of the new double borate $K_3Eu_3B_4O_{12}$. Kondens Sredy Mezhfaznye Granitsy. 2020;22:219–224. doi:10.17308/kcmf.2020.22/2823
9. Subanakov AK, Kovtunets EV, Bazarov BG, Dorzhieva SG, Bazarova JG. New double holmium borates: $Rb_3HoB_6O_{12}$ and $Rb_3Ho_2B_3O_9$. Solid State Sci. 2020;105. doi:10.1016/j.solidstatesciences.2020.106231
10. Subanakov AK, Kovtunets EV, Bazarov BG, Pugachev AM, Sofich DO, Bazarova JG. Exploration of structural, thermal and vibrational properties of new noncentrosymmetric double borate $Rb_3Tm_2B_3O_9$. Solid State Sci. 2021;120. doi:10.1016/j.solidstatesciences.2021.106719
11. Xia M, Shen S, Lu J, Sun Y, Li R. K3Li3Gd7(BO3)9: A New Gadolinium-Rich Orthoborate for Cryogenic Magnetic Cooling.

Chem – A Eur J. 2018;24:3147–3150. doi:10.1002/chem.201705669

12. Xia M, Zhai K, Lu J, Sun Y, Li RK. Orthoborates LiCdRE$_5$(BO$_3$)$_6$ (RE = Sm–Lu and Y) with Rare-Earth Ions on a Triangular Lattice: Synthesis, Crystal Structure, and Optical and Magnetic Properties. Inorg Chem. 2017;56:8100–8105. doi:10.1021/acs.inorgchem.7b00756

13. Xia M-J, Li RK. A new quaternary rare earth borate, CsLi$_2$Gd$_4$(BO$_3$)$_5$. Acta Crystallogr Sect E Struct Reports Online. 2007;63. doi:10.1107/S1600536807036586

14. Chen C, Wu Y, Li R. The development of new NLO crystals in the borate series. J Cryst Growth. 1990;99:790–798. doi:10.1016/S0022-0248(08)80028-0

15. Chen C, Li R. The anionic group theory of the non-linear optical effect and its applications in the development of new high-quality NLO crystals in the borate series. Int Rev Phys Chem. 1988;8:65–91. doi:10.1080/01442358909353223

16. Qin F, Li RK. Predicting refractive indices of the borate optical crystals. J Cryst Growth. 2011;318:642–644. doi:10.1016/J.JCRYSGRO.2010.08.037

17. Yu H, Pan Z, Zhang H, Wang J. Recent advances in self-frequency-doubling crystals. J Mater. 2016;2:55–65. doi:10.1016/j.jmat.2015.12.001

18. Jia Z, Xia M. Congruent melt terbium-rich borate Na$_2$Tb$_2$B$_2$O$_7$: Synthesis, crystal structure, optical and magnetic properties. J Alloys Compd. 2018;743:537–542. doi:10.1016/j.jallcom.2018.02.031

19. Shan F, Zhang G, Yao J, Xu T, Zhang X, Fu Y, et al. Growth, structure, and optical properties of a self-activated crystal: Na$_2$Nd$_2$O(BO$_3$)$_2$. Opt Mater (Amst). 2015;46:461–466. doi:10.1016/j.optmat.2015.05.004

20. Nagpure PA, Omanwar SK. Synthesis and photoluminescence study of rare earth activated phosphor Na$_2$La$_2$B$_2$O$_7$. J Lumin. 2012;132:2088–2091. doi:10.1016/j.jlumin.2012.03.068

21. Mascetti J, Fouassier C, Hagenmuller P. Concentration quenching of the Nd^{3+} emission in alkali rare earth borates. J Solid State Chem. 1983;50:204–212. doi:10.1016/0022-4596(83)90189-5

22. Wang Z, Li H, Cai G, Jin Z. Synthesis, crystal structure, and thermal stability of new borates Na$_3$REB$_2$O$_6$ (RE = Pr, Sm, Eu). Powder Diffr. 2016;31:110–117. doi:10.1017/S0885715616000051

23. Zhang Y, Chen XL, Liang JK, Xu T. Synthesis and structural study of new rare earth sodium borates Na$_3$Ln(BO$_3$)$_2$ (Ln=Y, Gd). J Alloys Compd. 2002;333:72–75. doi:10.1016/S0925-8388(01)01689-9

24. Zhang G, Wu Y, Fu P, Wang G, Liu H, Fan G, et al. A new sodium samarium borate Na$_3$Sm$_2$(BO$_3$)$_3$. J Phys Chem Solids. 2001;63:145–9. doi:10.1016/S0022-3697(01)00090-7

25. Yang Z, Ning Y, Keszler DA. Na$_3$Sc$_2$(BO$_3$)$_3$. Acta Crystallogr Sect E Struct Reports Online. 2006;62:266–268. doi:10.1107/S1600536806036737

26. Zhou WW, Zhuang RZ, Zhao W, Wang GF, Zhang LZ, Ma JG, et al. Second harmonic generation in Na$_3$Gd$_2$(BO$_3$)$_3$ crystals. Cryst Res Technol. 2011;46:926–930. doi:10.1002/crat.201100077

27. Shan F, Kang L, Zhang G, Yao J, Lin Z, Xia M, et al. Na$_3$Y$_3$(BO$_3$)$_4$: A new noncentrosymmetric borate with an open-framework structure. Dalt Trans. 2016;45:7205–7208. doi:10.1039/c6dt00950f

28. Gravereau P, Chaminade JP, Pechev S, Nikolov V, Ivanova D, Peshev P. Na$_3$La$_9$O$_3$(BO$_3$)$_8$, a new oxyborate in the ternary system Na$_2$O–La$_2$O$_3$–B$_2$O$_3$: Preparation and crystal structure. Solid State Sci. 2002. doi:10.1016/S1293-2558(02)01344-4

29. Zhang J, Zhang G, Li Y, Wu Y, Fu P, Wu Y. Thermophysical properties of a new nonlinear optical Na$_3$La$_9$O$_3$(BO$_3$)$_8$ crystal. Cryst Growth Des. 2010;10:4965–4967. doi:10.1021/cg1010743

30. Coelho AA. Topas: General Profile and Structure Analysis Software for Powder Diffraction Data. Bruker AXS, 2005.